IOP Publishing Physica Scripta
Phys. Scr. 95 (2020) 035209 (11pp) https://doi.org/10.1088/1402-4896/ab4ffb

Optimization of entropy generation in nonlinear stratified Powell–Eyring fluid with convective boundary conditions

Iffat Jabeen[1,2], M Farooq[1], N A Mir[1], S Ahmad[1] and Aisha Anjum[1]

[1] Department of Mathematics, Riphah International University, Islamabad 44000, Pakistan
[2] Department of Mathematics, COMSATS University Islamabad, Islamabad 44000, Pakistan

E-mail: iffatjabeen@comsats.edu.pk and iffatjabeen@yahoo.com

Received 19 June 2019, revised 21 September 2019
Accepted for publication 22 October 2019
Published 4 February 2020

Abstract

Entropy generation phenomenon is applied in reactors, turbines, natural convection, chillers, functional and regular graded materials. Irreversibility of a system and surroundings in Powell–Eyring fluid is analyzed in this research article. Flow is deformed by an inclined sheet. Measure of irreversibility is also called entropy. Rate of Entropy generation is calculated by considering heat transfer, radiation and viscous dissipation phenomena. Thermal stratification (nonlinear) and heat generation/absorption are incorporated in heat transport while solutal stratification (nonlinear) and chemical reaction have taken part in mass transport. Mixed convection phenomenon is also accounted here. To obtain the analytical solutions of nonlinear and non-dimensional governing equations homotopic analysis method is applied. The behavior of emerging parameters is discussed comprehensively via velocity, temperature and concentration profile. Entropy generation can be minimized by small values of Prandtl number and Eckert number. Thus, these physical phenomena can be used as a cooling agent in various industrial processes.

Keywords: Powell–Eyring, chemical reaction, inclined sheet, mixed convection, dual stratification, radiation, entropy generation

(Some figures may appear in colour only in the online journal)

Nomenclature

Ng	Entropy generation (non-dimensional)
u, v	Velocity component
C	Fluid concentration
C_0	Reference concentration
C_∞	Ambient concentration
C_f	Variable concentration
T	Fluid temperature
T_0	Reference temperature
T_∞	Ambient temperature
T_f	Heated fluid temperature
C_{fx}	Skin friction coefficient
Q_0	Heat generation/Absorption coefficient
u_w	Stretching velocity
β, C_1	Material parameters
Sh_x	Sherwood number
R	Radiation parameter
Ec	Eckert number
Be	Bejan number
D	Diffusion species coefficient
Nu_x	Nusselt number
R_e	Reynolds number
Sc	Schmidt number
Pr	Prandtl number

C_p	Specific heat capacity
d_1, d_2, e_1, e_2	Dimensional constant
h_f	Heat transfer coefficient
h_c	Mass transfer coefficient
S_1	Thermal stratification parameter
S_2	Solutal stratification parameter
g	Gravitational acceleration
k	Thermal conductivity
kr	Chemical reaction parameter
K_1	Chemical reaction coefficient

Greek symbols

υ	Kinematic viscosity
δ, ε	Dimensionless parameters
ξ	Similarity variable
φ	Dimensionless concentration
λ	Thermal buoyancy parameter
λ_1	Solutal buoyancy parameter
γ_1	Thermal Biot number
θ	Dimensionless temperature
ρ	Fluid density
k^*	Absorption coefficient
b	Diffusion variable
δ_1	Heat generation/absorption parameter
γ_2	Solutal Biot number
β_1	Angle of inclination
β_T	Coefficient of thermal expansion
β_C	Coefficient of mass expansion

1. Introduction

For best utilization of energy during fluid flow entropy generation is introduced and it is used to find out the destruction in the performance of the system. Only in irreversible process entropy production is applied not for reversible processes e.g. chemical reaction, Joule heating, diffusion, friction between fluid surfaces. To increase the efficiency of thermal equipments minimization of entropy generation is must. Entropy generation processes are applied in gas turbines, reactors, chillers, fuel cells, air seperators, curved pipes, evaporative cooling, natural convection, solar thermal, functional and regular graded materials. According to the previous research survey researchers did alot of work on entropy generation. Khan *et al* [1] have discussed the impact of entropy generation on viscous fluid with radiation and binary chemical reaction effects. Khan *et al* [2] disclosed the features of entropy optimization in chemically reactive Williamson nanofluid with Joule heating. Alharbi *et al* [3] considered Powell–Eyring fluid to elaborate the effects of Entropy generation with MHD and radiation effect. Jamshed *et al* [4] have analyzed the entropy in Powell–Eyring nanofluid with variable thermal conductivity and thermal radiation. Butt *et al* [5–7] have elaborated the entropy generation effects in a magnetohydrodynamic nanofluid flow deformed by a stretching sheet in the presence of viscous dissipation and radiation.

Several models for non-Newtonian fluids have been introduced by the scientists to explore the features of heat transfer and fluid flow. One of the models is known as Powell–Eyring model for non-Newtonian fluids. Scientists adopted this model because it has two main advantages over other models (i) it is derived from kinetic theory of gases instead of empirical formula (ii) It behaves like Newtonian fluid at high or low shear stresses. It has many applications in industrial and natural processes, agricultural field, thermal insulation, thermal radiation, environmental pollution and geo thermal reservoirs. Hayat *et al* [8] discussed the Powell–Eyring fluid with the effect of non-Fourier heat flux theory. Adesanyaa *et al* [9] discussed the squeezing flow in Powell–Eyring fluid with radiation and chemical reaction. Rehman *et al* [10] analyzed the effects of stratification and mixed convection in Powell–Eyring fluid flow. Rehman *et al* [11] have analyzed the Powell–Eyring fluid flow in the presence of stagnation point. Rahimi *et al* [12] used collocation method to analyze the effects of Powell–Eyring fluid over a stretching sheet.

In many engineering problems internal heat generation or absorption occurs. In this manner, Hayat *et al* [13] have described the effects of heat generation/absorption in three-dimensional viscoelastic nanofluid. Hayat *et al* [14] have checked the heat generation/absorption effects in Walters-B nanofluid in the presence of Cattaneo–Christov model. Soomro *et al* [15] have analyzed the effects of heat generation/absorption in the presence of stagnation point with nonlinear radiation. Qayyum *et al* [16] have elaborated the heat generation/absorption effects over a stretching sheet in third grade nanofluid. Anjum *et al* [17] explained the heat generation/absorption effects in second grade fluid deformed by a Riga plate.

Five novel aspects are there in our present research. Firstly Powell–Eyring fluid flow is applied by inclined stretching sheet with convective boundary conditions. Secondly, we analyzed heat transfer with Entropy generation along with dual stratification (nonlinear). Thirdly heat transfer is also helped out with heat generation/absorption and radiation. Fourthly mass transfer is carried out with chemical reaction. Fifthly to find out solution of convergent series solution homotopic analysis method [18–24] is used and arising dominating parameters are discussed by plots. Features of skin friction, Nusselt number and Sherwood number are also elaborated through graph.

In the abovementioned studies, no one has attempted the study of Powell–Eyring fluid on two-dimensional flow with nonlinear stratification over a stretchable inclined surface in collaboration with entropy generation and convective heat and mass boundary conditions. Hence to fill this breach is our basic theme.

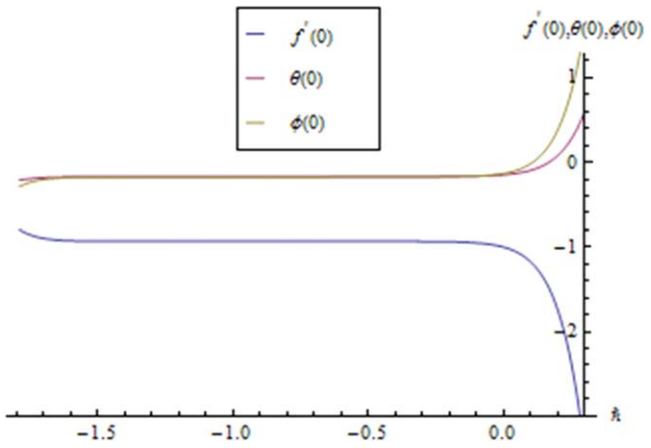

Figure 1. h-curves for $f(\xi)$, $\theta(\xi)$, $\phi(\xi)$.

2. Mathematical modeling

We consider Powell–Eyring fluid flow (incompressible and steady) persuaded by linearly stretchable sheet inclined at an angle β_1 with the horizontal line. Mixed convective phenomena is applied to demonstrate the features of allied mass and heat transport. Nonlinear stratification is also implemented in order to analyze heat and mass flux. Heat generation/absorption and thermal radiation assisted heat transfer phenomena. Entropy generation is also implemented. Mass transfer mechanism is evaluated in the light of constructive and destructive chemical reactions. The governing equations by implementing boundary layer approximations are as follows [25, 26]:

$$\frac{\partial u}{\partial x}+\frac{\partial v}{\partial y}=0, \tag{1}$$

$$u\frac{\partial u}{\partial x}+v\frac{\partial u}{\partial y}=\left(\upsilon+\frac{1}{\rho\beta C_1}\right)\frac{\partial^2 u}{\partial y^2}-\frac{1}{2\rho\beta C_1^3}\left(\frac{\partial u}{\partial y}\right)^2 \times\frac{\partial^2 u}{\partial y^2}+\begin{pmatrix}(\beta_T(T-T_\infty)+\\ \beta_C(C-C_\infty)\end{pmatrix}g\sin\beta_1, \tag{2}$$

$$u\frac{\partial T}{\partial x}+v\frac{\partial T}{\partial y}=\frac{k}{\rho c_p}\frac{\partial^2 T}{\partial y^2}+\frac{Q_0}{\rho c_p}(T-T_0)+\frac{16\sigma^*}{\rho c_p 3k^*}\times T_\infty^3\frac{\partial^2 T}{\partial y^2}+\left(\mu+\frac{1}{\beta C_1}\right)\left(\frac{\partial u}{\partial y}\right)^2-\frac{1}{6\beta C_1^3}\left(\frac{\partial u}{\partial y}\right)^4, \tag{3}$$

$$u\frac{\partial C}{\partial x}+v\frac{\partial C}{\partial y}=K_1(C-C_\infty)+D\frac{\partial^2 C}{\partial y^2}, \tag{4}$$

with the boundary conditions [27, 28]:

$$u=u_w(x)=cx,\ -k\frac{\partial T}{\partial y}=h_f(T_w-T),\ -D\frac{\partial C}{\partial y}=h_c(C_w-C),\ v=0,\ \text{at } y=0,$$
$$u\to 0,\ T\to T_\infty(x),\ C\to C_\infty(x)\ \text{as } y\to\infty, \tag{5}$$

where

$$T_w(x)=T_0+d_1x^2,\ C_w(x)=C_0+e_1x^2,\ T_\infty(x)=T_0+d_2x^2,\ C_\infty(x)=C_0+e_2x^2, \tag{6}$$

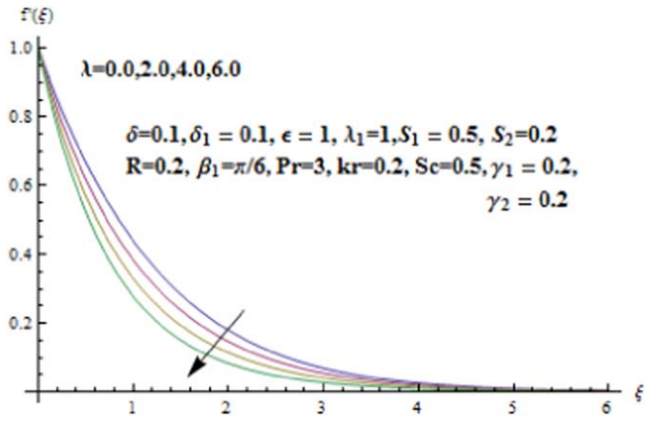

Figure 2. Analysis of λ on $f'(\xi)$.

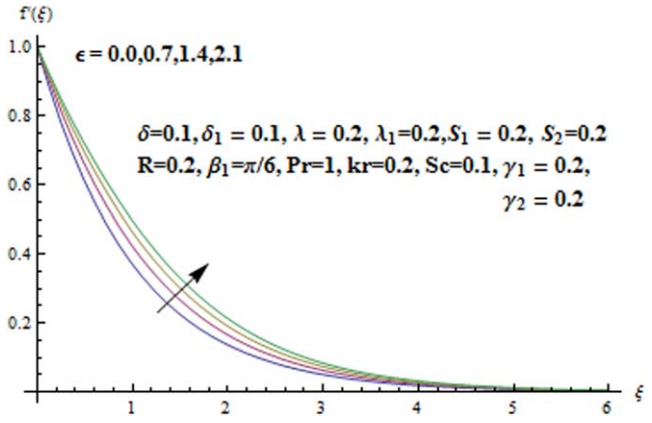

Figure 3. Analysis of ε on $f'(\xi)$.

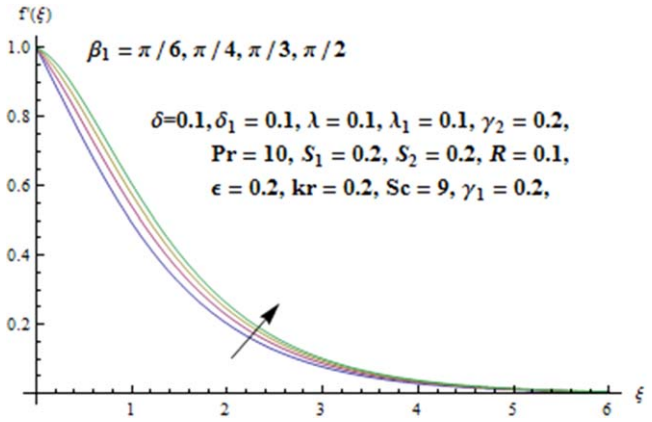

Figure 4. Analysis of β_1 on $\theta(\xi)$.

In above expressions, υ represents fluid kinematic viscosity, u_w represents stretching velocity, ρ represents density, T_w the stretching temperature of fluid, thermal expansion is represented by β_T, g stands for gravitational acceleration, T_∞ the variable ambient fluid temperature, C_w the stretching concentration of heated fluid, β_1 represents angle of inclination, C_1 and β are material parameters, β_C represents coefficient of mass expansion, C_∞ the variable ambient concentration, specific heat is demonstrated by C_p, K_1 is chemical reaction coefficient, h_f and h_c demonstrate heat and

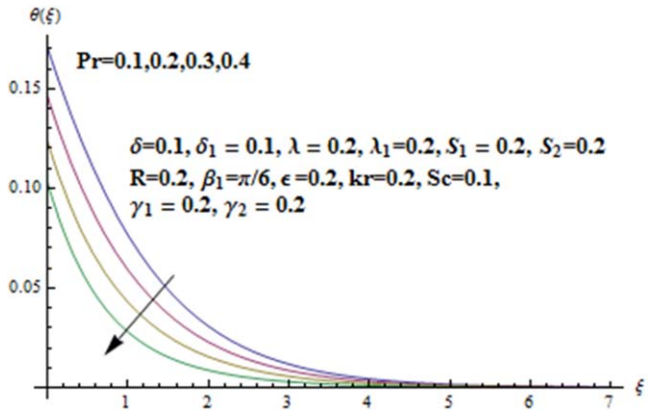

Figure 5. Analysis of Pr on $\theta(\xi)$.

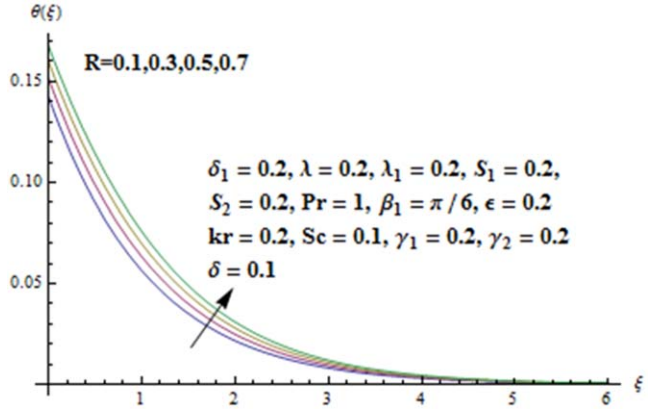

Figure 6. Analysis of R on $\theta(\xi)$.

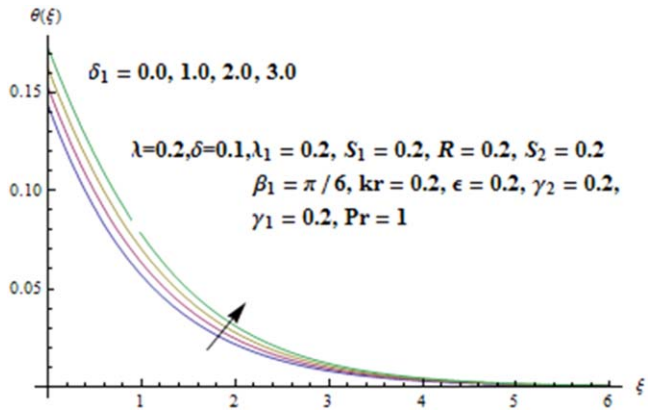

Figure 7. Analysis of δ_1 on $\theta(\xi)$.

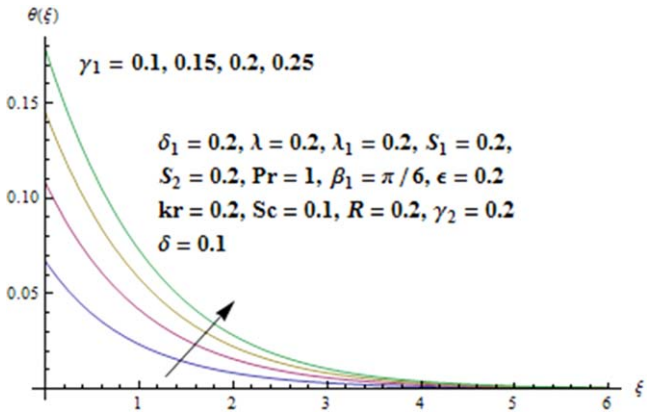

Figure 8 Analysis of γ_1 on $\theta(\xi)$.

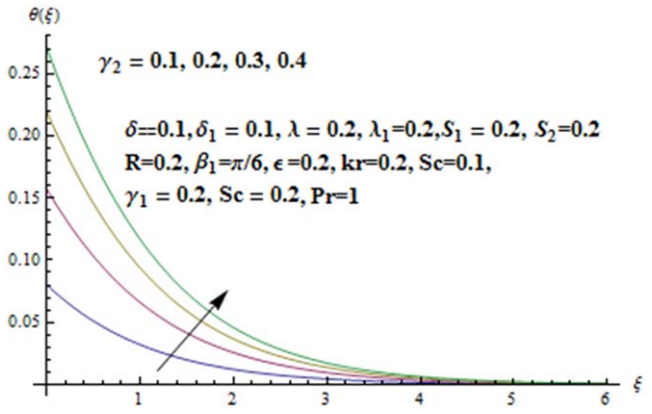

Figure 9. Analysis of γ_2 on $\varphi(\xi)$.

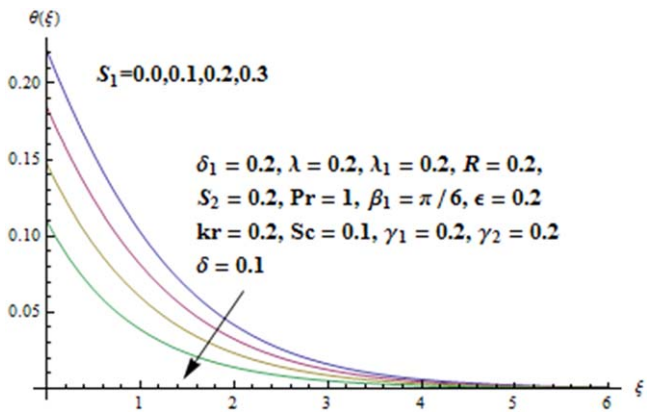

Figure 10. Analysis of S_1 on $\theta(\xi)$.

mass transfer coefficients, T_0 and C_0 represent reference temperature and concentration respectively, D is diffusion species coefficient, σ^* Stephen Boltzmann constant and concentration, Q_0 is heat generation/absorption coefficient, k^* absorption coefficient, d_1, d_2, e_1, and e_2 represents dimensional constants and k represents thermal conductivity. It is noted that $u_w(x) = cx$ at $y = 0$ represents stretching velocity which is produced by applying two forces of same magnitude but in opposite direction in order origin is kept constant, $v = 0$ demonstrates that plate is impermeable, $-k\frac{\partial T}{\partial y} = h_f(T_w - T)$ is a convective boundary condition due to temperature which is derived from Newton's law of cooling and Fourier law of heat conduction, $-D\frac{\partial C}{\partial y} = h_c(C_w - C)$ is a convective boundary condition due to concentration and is derived from Fick's first and second laws, $u \to \infty$ velocity outside the boundary layer and approaches to zero while temperature and concentration approaches to $T_\infty(x)$ and $C_\infty(x)$ respectively, which vary quadratically, as we move away from the origin and these temperature and

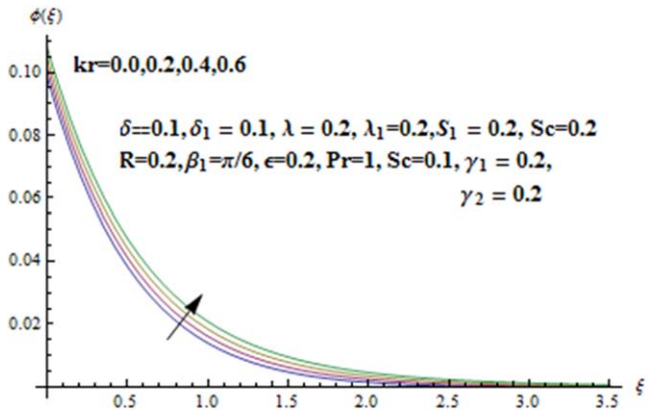

Figure 11. Analysis of kr on $\varphi(\xi)$.

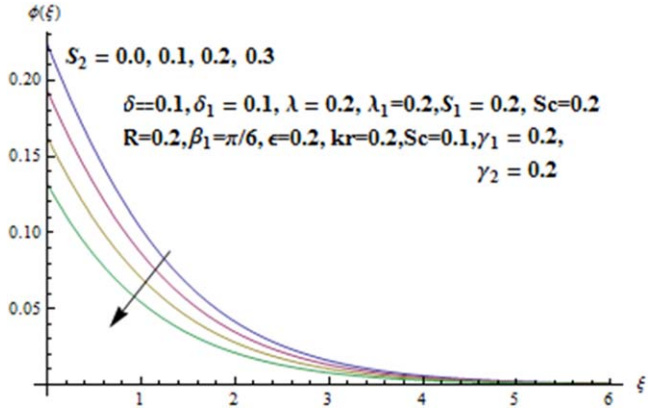

Figure 12. Analysis of S_2 on $\varphi(\xi)$.

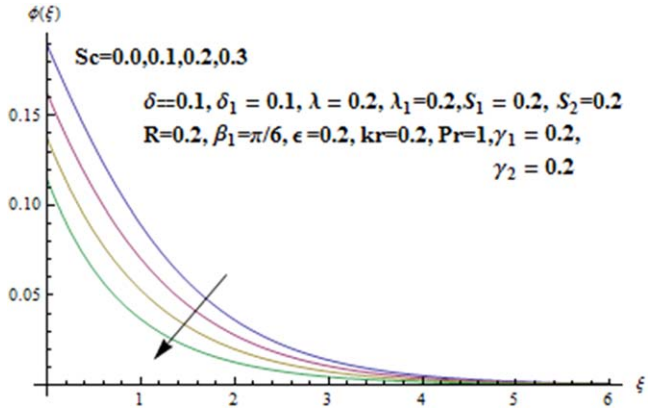

Figure 13. Analysis of Sc on $\varphi(\xi)$.

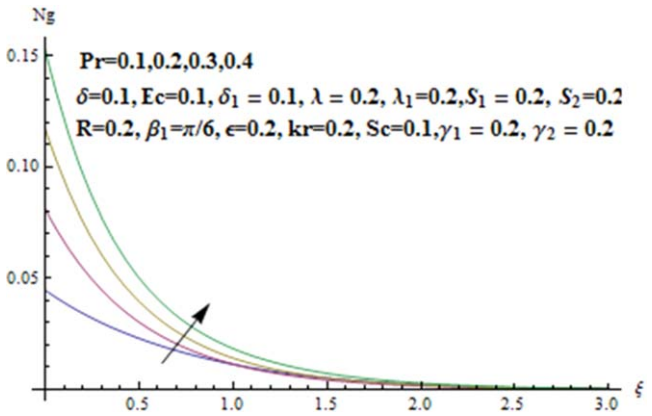

Figure 14. Analysis of Pr on Ng.

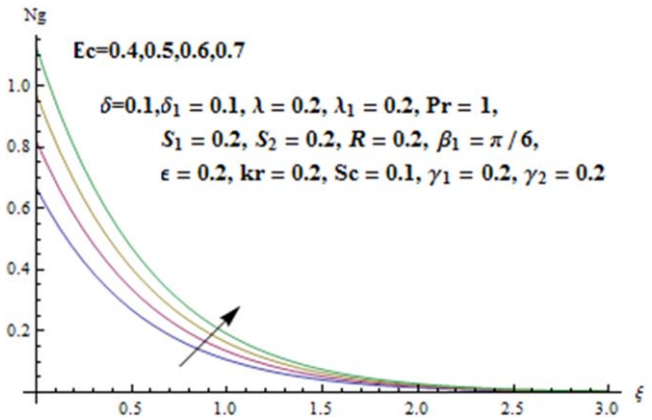

Figure 15. Analysis of Ec on Ng.

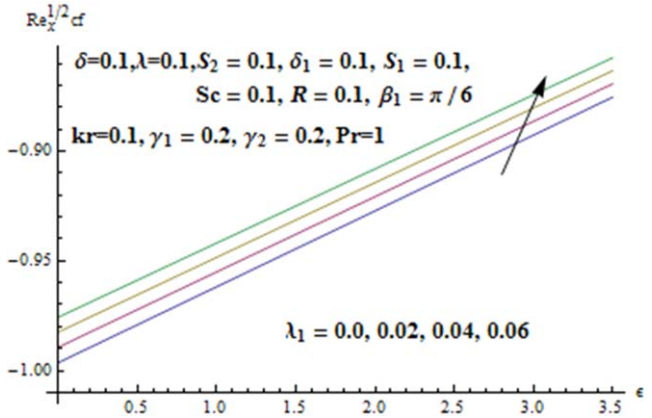

Figure 16. Analysis of λ_1 and ε on Cf.

concentration fields are responsible for thermal solutal stratifications.

Implementing the transformations [28, 29]

$$\xi = y\sqrt{\frac{c}{\upsilon}},\ u = cxf'(\xi),\ v = -\sqrt{c\upsilon}f(\xi),$$
$$\theta(\xi) = \frac{T - T_\infty}{T_w - T_0},\ \varphi(\xi) = \frac{C - C_\infty}{C_w - C_0}, \tag{7}$$

The continuity equation equation (1) vanishes, while equations (2)–(4) take the forms:

$$(1 + \varepsilon)f''' + ff'' - f'^2 - \varepsilon\delta f''^2 f''' + \lambda\theta \sin\beta_1 + \lambda_1\varphi \sin\beta_1 = 0, \tag{8}$$

$$\theta''(1 + R) - 2f'S_1Pr - 2f'\theta Pr + \theta' fPr + \delta_1\theta Pr + Ec\left[(1 + \varepsilon)f''^2 - \frac{1}{3}\varepsilon\delta f''^4\right] = 0, \tag{9}$$

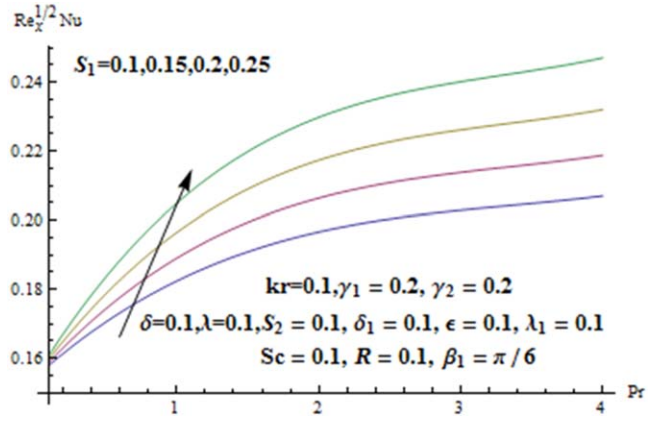

Figure 17. Analysis of S_1 and Pr on Nu.

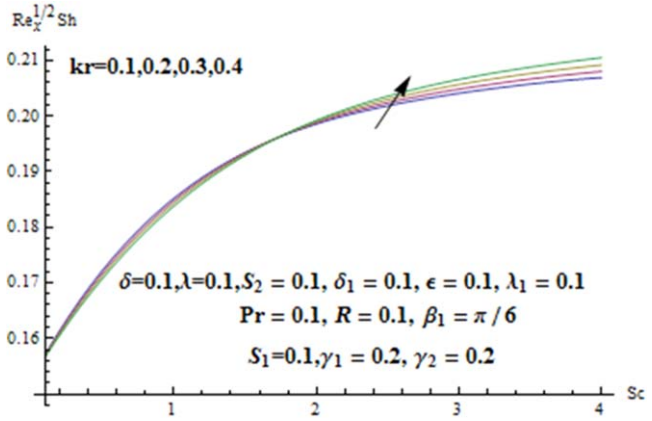

Figure 18. Analysis of kr and Sc on Sh.

$$\varphi'' - Sc(2S_2 f' + 2f'\varphi - f\varphi') + Sckr\varphi = 0, \tag{10}$$

Dimensionless boundary conditions are:

$$\begin{aligned} &f'(0) = 1,\ f(0) = 0,\ \theta'(0) = -\gamma_1(1 - S_1 - \theta(0)),\\ &\varphi'(0) = -\gamma_2(1 - S_2 - \varphi(0)),\\ &f'(\infty) = 0,\ \theta(\infty) = 0,\ \varphi(\infty) = 0, \end{aligned} \tag{11}$$

where Sc represents Schmidt number, Ec is Eckert number, R is radiation parameter, dimensionless material parameter are ε and δ, γ_1 is Biot number (thermal), λ_1 is solutal buoyancy parameter, Prandtl number is represented by, S_2 and S_1 represent solutal and thermal stratified parameters, γ_2 is solutal Biot number, β_1 is an angle of inclination, λ is thermal buoyancy parameter, kr represents chemical reaction parameter and δ_1 is heat generation/absorption parameter. These dimensionless parameters are expressed as given below:

$$\begin{aligned} &Pr = \frac{\upsilon}{\alpha},\ \varepsilon = \frac{1}{\mu\beta C_1},\ \delta = \frac{x^2c^3}{2\upsilon C_1^2},\ kr = \frac{K_1}{c},\ Sc = \frac{\upsilon}{D},\\ &\lambda = \frac{g\beta_T(T_w - T_0)}{xc^2},\ \lambda_1 = \frac{g\beta_C(C_w - C_0)}{xc^2},\ S_1 = \frac{d_2}{d_1},\\ &S_2 = \frac{e_2}{e_1},\ \gamma_1 = \frac{h_f}{k\sqrt{\frac{c}{\upsilon}}},\ \gamma_2 = \frac{h_c}{D\sqrt{\frac{c}{\upsilon}}},\\ &R = \frac{16\sigma^*}{3kk^*}T_\infty^3,\ \delta_1 = \frac{Q_0}{\rho C_p c},\ Ec = \frac{c^2}{d_1 C_p}, \end{aligned} \tag{12}$$

Surface drag force is as follows:

$$C_{fx} = \frac{\tau_w}{\rho u_w^2}, \tag{13}$$

where wall shear stress

$$\begin{aligned} &\tau_w = \tau_{xy} = \left(\mu + \frac{1}{\beta C_1}\right)\left(\frac{\partial u}{\partial y}\right) - \frac{1}{6\beta C_1^3}\left(\frac{\partial u}{\partial y}\right)^3,\\ &C_f Re_x^{1/2} = (1 + \varepsilon)f''(0) - \frac{\varepsilon}{3}\delta f''^3(0). \end{aligned} \tag{14}$$

Nusselt number is as follows:

$$\begin{aligned} &Nu_x = \frac{xq_w}{k(T_f - T_\infty)},\\ &q_w = -k\left(\frac{\partial T}{\partial y}\right),\\ &Nu_x = \frac{-\theta'(0)}{Re_x^{-1/2}(1 - S_1)}. \end{aligned} \tag{15}$$

Sherwood number is as follows:

$$\begin{aligned} &Sh_x = \frac{xq_m}{D(C_f - C_\infty)},\ q_m = -D\left(\frac{\partial C}{\partial y}\right),\\ &Sh_x = \frac{-\varphi'(0)}{Re_x^{-1/2}(1 - S_2)}. \end{aligned} \tag{16}$$

Reynolds number is represented by $Re_x = \frac{u_w x}{\upsilon}$.

2.1. Entropy generation modeling

Here total Entropy generation rate is calculated by second law of thermodynamics. Rate of entropy generation is calculated by heat transfer, thermal radiation and viscous dissipation and chemical reaction. In thermal engineering most recent investigation reports that second law of thermodynamics [30] is more significant than first law of thermodynamics. The main difference is that first law provides only accounting or quantity of energy while second law provides variation as well as direction of heat transfer. Bejan [31, 32] is the first who studied entropy generation in a convective heat transfer problems

$$Eg = (Eg)_T + (Eg)_R + (Eg)_{\tau.L} + (Eg)_{kr}, \tag{17}$$

$$\begin{aligned} Eg = &\frac{k}{(T_\infty - T_0)^2}\left(\frac{\partial T}{\partial y}\right)^2 + \frac{k}{(T_\infty - T_0)^2}\left(\frac{16\sigma^*}{3k^*}T_\infty^3\right)\\ &\times\left(\frac{\partial T}{\partial y}\right)^2 + \frac{\tau.L}{T_\infty - T_0} + \frac{D}{C_\infty - C_0}\left(\frac{\partial C}{\partial y}\right), \end{aligned} \tag{18}$$

$$Eg_0 = \frac{(T_\infty - T_0)^2\left(\frac{y}{\eta}\right)^2}{k(T_w - T_\infty)^2}, \tag{19}$$

Table 1. Comparison of skin friction coefficient $C_f Re_x^{1/2}$ of the present values [in brackets] with the previous published results Javed *et al* and (Wahab *et al*) for $\lambda = 0$ and $\lambda_1 = 0$

ε/δ	0.0	0.2	0.4	0.6	0.8	1.0
0.0	−1	−1.0954	−1.1832	−1.2649	−1.3416	−1.4142
	(−1)	(−1.095 445)	(−1.264 911)	(−1.264 911)	(−1.341 641)	(−1.414 214)
	[−1]	[−1.095 45]	[−1.264 92]	[−1.264 910]	[−1.341 639]	[−1.414 213]
0.1	−1	−1.0940	−1.1808	−1.2620	−1.3384	−1.4107
	(−1)	(−1.093 953)	(−1.188 42)	(−1.261 993)	(−1.338 379)	(−1.410 732)
	[−1]	[−1.093 951]	[−1.188 42]	[−1.261 991]	[−1.338 377]	[−1.410 730]
0.2	−1	−1.0924	−1.1784	−1.2590	−1.3351	−1.4072
	(−1)	(−1.092 445)	(−1.178 431)	(−1.259 022)	(−1.335 054)	(−1.407 183)
	[−1]	[−1.092 443]	[−1.178 429]	[−1.259 020]	[−1.335 054]	[−1.407 183]
0.3	−1	−1.0909	−1.1776	−1.2560	−1.3317	−1.4036
	(−1)	(−1.090 921)	(−1.175 981)	(−1.255 996)	(−1.331 665)	(−1.403 562)
	[−1]	[−1.090 920]	[−1.175 979]	[−1.255 994]	[−1.331 663]	[−1.403 561]
0.4	−1	−1.0894	−1.1735	−1.2529	−1.3282	−1.3999
	(−1)	(−1.089 381)	(−1.173 490)	(−1.252 912)	(−1.328 205)	(−1.399 867)
	[−1]	[−1.089 380]	[−1.173 490]	[−1.252 910]	[−1.328 203]	[−1.399 865]
0.5	−1	−1.0878	−1.1710	−1.2498	−1.3247	−1.3961
	(−1)	(−1.087 823)	(−1.170 957)	(−1.249 765)	(−1.324 671)	(−1.396 090)
	[−1]	[−1.087 821]	[−1.170 955]	[−1.249 763]	[−1.324 669]	[−1.396 089]
0.6	−1	−1.0862	−1.1684	−1.2466	−1.3211	−1.3922
	(−1)	(−1.086 247)	(−1.168 379)	(−1.246 551)	(−1.321 057)	(−1.392 28)
	[−1]	[−1.086 247]	[−1.168 377]	[−1.246 550]	[−1.246 551]	[−1.392 28]
0.7	−1	−1.0847	−1.1658	−1.2433	−1.3174	−1.3883
	(−1)	(−1.084 653)	(−1.165 752)	(−1.243 67)	(−1.317 359)	(−1.388 272)
	[−1]	[−1.084 653]	[−1.165 752]	[−1.243 66]	[−1.317 357]	[−1.388 270]
0.8	−1	−1.0830	−1.1631	−1.2399	−1.3136	−1.3842
	(−1)	(−1.083 040)	(−1.163 075)	(−1.239 906)	(−1.313 568)	(−1.384 217)
	[−1]	[−1.083 039]	[−1.163 073]	[−1.239 902]	[−1.313 565]	[−1.384 217]
0.9	−1	−1.0814	−1.1603	−1.2365	−1.3097	−1.3801
	(−1)	(−1.081 407)	(−1.160 345)	(−1.236 464)	(−1.309 677)	(−1.388 0053)
	[−1]	[−1.081 405]	[−1.160 343]	[−1.236 463]	[−1.309 677]	[−1.388 0053]
1.0	−1	−1.0798	−1.1576	−1.2329	−1.3057	−1.3758
	(−1)	(−1.079 753)	(−1.157 556)	(−1.232 933)	(−1.305 679)	(−1.375 771)
	[−1]	[−1.079 750]	[−1.157 555]	[−1.232 931]	[−1.305 677]	[−1.375 769]

$$Ng = \frac{Eg}{Eg_0}. \tag{20}$$

Non-dimensional form of Entropy generation is:

$$Ng = \frac{(\theta')^2}{(1 - S_1)^2} + R\frac{(\theta')^2}{(1 - S_1)^2} + PrEc\frac{S_1^2}{(1 - S_1)^2} \times \left[(1 + \varepsilon)f''^2 + \frac{1}{3}\varepsilon\delta f''^4\right] + \frac{\varphi'^2 S_1^2 b}{S_2(1 - S_1)^2}, \tag{21}$$

where, first term on right-hand side shows entropy generation due to heat transfer, second term represents entropy generation due to radiation, third term shows entropy generation because of viscous dissipation and last term shows entropy generation due to chemical reaction.

$Pr\left(=\frac{\mu C_p}{k}\right)$ represents Prandtl number,

$Ec\left(=\frac{c^2}{(T_\infty - T_0)C_p}\right)$is Eckert number,

$R\left(=\frac{16\sigma^*}{3kk^*}T_\infty^3\right)$is radiation parameter,

$b\left(=\frac{De_1}{k}\right)$is diffusion variable. (22)

Bejan number is expressed as:

$$Be = \frac{\text{Heat transfer irreversibility}}{\text{Total entropy}}, \tag{23}$$

$$Be = \frac{\frac{(\theta')^2}{(1 - S_1)^2}}{\frac{(\theta')^2}{(1 - S_1)^2} + R\frac{(\theta')^2}{(1 - S_1)^2} + PrEc\frac{S_1^2}{(1 - S_1)^2}\left[(1 + \varepsilon)f''^2 + \frac{1}{3}\varepsilon\delta f''^4\right] + \frac{\varphi'^2 S_1^2 b}{S_2(1 - S_1)^2}}. \tag{24}$$

3. Analytical method of solution

To find out analytical solutions of nonlinear differential equations (8)–(10), homotopic analysis method is implemented. Nonlinear (weak or strong) mathematical problems are well solved by this technique because it is independent of large or small parameters. There is no restriction of choosing the initial guesses and linear operators to obtain the analytical solution of series.

The initiatory guesses are:

$$\begin{aligned} f_0(\xi) &= 1 - \exp(-\xi), \\ \theta_0(\xi) &= \frac{(1 - S_1)\gamma_1}{1 + \gamma_1}\exp(-\xi), \\ \varphi_0(\xi) &= \frac{(1 - S_2)\gamma_2}{1 + \gamma_2}\exp(-\xi), \end{aligned} \tag{25}$$

Corresponding linear operators are:

$$\begin{aligned} L_f(f) &= \frac{\mathrm{d}^3 f}{\mathrm{d}\xi^3} - \frac{\mathrm{d}f}{\mathrm{d}\xi}, \\ L_\theta(\theta) &= \frac{\mathrm{d}^2\theta}{\mathrm{d}\xi^2} - \theta, \\ L_\varphi(\varphi) &= \frac{\mathrm{d}^2\varphi}{\mathrm{d}\xi^2} - \varphi, \end{aligned} \tag{26}$$

which satisfy the specified properties

$$\begin{aligned} &L_f[A_3\exp(-\xi) + A_2\exp(\xi) + A_1] = 0, \\ &L_\theta[A_5\exp(-\xi) + A_4\exp(\xi)] = 0, \\ &L_\varphi[A_7\exp(-\xi) + A_6\exp(\xi)] = 0, \end{aligned} \tag{27}$$

where $A_i (i = 1 - 7)$ are the optional constants.

3.1. Zeroth-order problems

$$\begin{aligned} &(1 - q)L_f[\tilde{f}(\xi; q) - f_0(\xi)] \\ &\quad = q\hbar_f N_f[\tilde{f}(\xi; q),\ \tilde{\theta}(\xi; q),\ \tilde{\varphi}(\xi; q)], \end{aligned} \tag{28}$$

$$\begin{aligned} &(1 - q)L_\theta[\tilde{\theta}(\xi; q) - \tilde{\theta}_0(\xi)] \\ &\quad = q\hbar_\theta N_\theta[\tilde{\theta}(\xi; q),\ \tilde{f}(\xi; q)], \end{aligned} \tag{29}$$

$$\begin{aligned} &(1 - q)L_\varphi[\tilde{\varphi}(\xi; q) - \tilde{\varphi}_0(\xi)] \\ &\quad = q\hbar_\varphi N_\varphi[\tilde{\varphi}(\xi; q),\ \tilde{f}(\xi; q),], \end{aligned} \tag{30}$$

$$\begin{aligned} &\tilde{f}'(0; q) = 1,\ \tilde{f}(0; q) = 0,\ \tilde{\theta}'(0; q) = -\gamma_1[1 - \tilde{\theta}(0) - S_1], \\ &\tilde{\varphi}'(0; q) = -\gamma_2[1 - \tilde{\varphi}(0) - S_2],\ \tilde{f}'(\infty; q) = 0, \\ &\tilde{\theta}(\infty; q) = 0,\ \tilde{\varphi}(\infty; q) = 0, \end{aligned} \tag{31}$$

$$\begin{aligned} N_f[\tilde{f}(\xi, q),\ \tilde{\theta}(\xi; q),\ \tilde{\varphi}(\xi; q)] &= (1 + \varepsilon)\frac{\partial^3\tilde{f}(\xi; q)}{\partial\xi^3} \\ &+ \tilde{f}(\xi, q)\frac{\partial^2\tilde{f}(\xi; q)}{\partial\xi^2} + \left(\frac{\partial\tilde{f}(\xi; q)}{\partial\xi}\right)^2 \\ &- \varepsilon\delta\left(\frac{\partial^2\tilde{f}(\xi; q)}{\partial\xi^2}\right)^2\frac{\partial^3\tilde{f}(\xi; q)}{\partial\xi^3} + \lambda\tilde{\theta}(\xi, q)\sin\beta_1 \\ &+ \lambda_1\tilde{\varphi}(\xi, q)\sin\beta_1, \end{aligned} \tag{32}$$

$$\begin{aligned} N_\theta[\tilde{f}(\xi, q),\ \tilde{\theta}(\xi; q),] &= (1 + R)\frac{\partial^2\tilde{\theta}(\xi; q)}{\partial\xi^2} \\ &- 2S_1 Pr\frac{\partial\tilde{f}(\xi; q)}{\partial\xi} - 2\tilde{\theta}(\xi, q)Pr\frac{\partial\tilde{f}(\xi; q)}{\partial\xi} \\ &+ Pr\,\tilde{f}(\xi, q)\frac{\partial\tilde{\theta}(\xi; q)}{\partial\xi} + \delta_1 Pr\,\tilde{\theta}(\xi, q) \\ &+ Ec\left[\begin{array}{l}(1 + \varepsilon)\left(\dfrac{\partial^2\tilde{f}(\xi; q)}{\partial\xi^2}\right)^2 \\ -\dfrac{1}{3}\varepsilon\delta\left(\dfrac{\partial^2\tilde{f}(\xi; q)}{\partial\xi^2}\right)^4\end{array}\right], \end{aligned} \tag{33}$$

$$\begin{aligned} N_\varphi[\tilde{f}(\xi, q),\ \tilde{\varphi}(\xi; q),] &= \frac{\partial^2\tilde{\varphi}(\xi; q)}{\partial\xi^2} \\ &- Sc\left[\begin{array}{c}2S_2\dfrac{\partial\tilde{f}(\xi; q)}{\partial\xi} + 2\dfrac{\partial\tilde{f}(\xi; q)}{\partial\xi}\tilde{\varphi}(\xi; q) \\ -\dfrac{\partial\tilde{f}(\xi; q)}{\partial\xi}\dfrac{\partial\tilde{\varphi}(\xi; q)}{\partial\xi}\end{array}\right] \\ &+ Sckr\tilde{\varphi}(\xi, q), \end{aligned} \tag{34}$$

[0, 1] represents the value of embedding parameter q while $\hbar_f$, $\hbar_\theta$, and $\hbar_\varphi$ are known as auxiliary parameters containing non-zero values.

3.2. mth-order problems

$$\begin{aligned} \hbar_f R_m^f(\xi) &= L_f[f_m(\xi) - \chi_m f_{m-1}(\xi)], \\ \hbar_\theta R_m^\theta(\xi) &= L_\theta[\theta_m(\xi) - \chi_m\theta_{m-1}(\xi)], \\ \hbar_\varphi R_m^\varphi(\xi) &= L_\varphi[\varphi_m(\xi) - \chi_m\varphi_{m-1}(\xi)], \end{aligned} \tag{35}$$

$$\begin{aligned} &f_m'(0) = 0,\ f(0) = 0,\ \theta_m'(0) = \gamma_1\theta_m(0), \\ &\varphi_m'(0) = -\gamma_2\varphi_m(0), f_m'(\infty) = 0,\ \theta_m(\infty) = 0, \\ &\varphi_m(\infty) = 0, \end{aligned} \tag{36}$$

$$\begin{aligned} R_m^f(\xi) &= (1 + \varepsilon)f_{m-1}''' + \sum_{k=0}^{m-1} f_{m-1-k}'''f_k - f_{m-1}'^2 \\ &- \varepsilon\delta\sum_{k=0}^{m-1} f_{m-1-k}'''\sum_{l=0}^{k} f_{k-l}''f_l'' + \lambda\sin\beta_1\theta_{m-1} \\ &+ \lambda_1\sin\beta_1\varphi_{m-1}, \end{aligned} \tag{37}$$

$$\begin{aligned} R_m^\theta(\xi) &= (1 + R)\theta_{m-1}'' - 2S_1 Pr\,f_{m-1}' \\ &-2Pr\sum_{k=0}^{m-1}(f_{m-1-k}'\theta_k) + \delta_1 Pr\,\theta_{m-1} \\ &+Ec\left[(1 + \varepsilon)\sum_{l=0}^{K}(f_{k-l}''f_l'')^2 - \frac{1}{3}\varepsilon\delta\sum_{k}^{l=0}(f_{k-l}''f_l'')^4\right] \\ &+Pr\sum_{k=0}^{m-1}(\theta_{m-1-k}'f_k), \end{aligned} \tag{38}$$

$$\begin{aligned} R_m^\varphi(\xi) &= \varphi_{m-1}'' - Sc\left[2S_2 f_{m-1}' + 2\sum_{k=0}^{m-1} f_{m-1-k}'\varphi_k\right. \\ &\left.-\sum_{k=0}^{m-1}\varphi_{m-1-k}'f_k\right] + Sckr\varphi_{m-1} \end{aligned} \tag{39}$$

$$\chi_m = \begin{cases} 0, & m \leqslant 1 \\ 1, & m > 1 \end{cases}. \tag{40}$$

For $q = 0$ and $q = 1$, one can write

$$f(\xi; 0) = f_0(\xi),\ f(\xi; 1) = f(\xi),$$
$$\theta(\xi; 0) = \theta_0(\xi),\ \theta(\xi; 1) = \theta(\xi),$$
$$\varphi(\xi; 0) = \varphi_0(\xi),\ \varphi(\xi; 1) = \varphi(\xi), \tag{41}$$

and with diversity of q from zero to one solution begins from first approximations $f_0(\xi)$, $\theta_0(\xi)$ and $\varphi_0(\xi)$ to final solutions. By using $q = 1$ and Taylor's series, we get

$$f(\xi) = f_0(\xi) + \sum_{m=1}^{\infty} f_m(\xi),\ \theta(\xi) = \theta_0(\xi)$$
$$+\sum_{m=1}^{\infty} \theta_m(\xi),\ \varphi(\xi) = \varphi_0(\xi) + \sum_{m=1}^{\infty} \varphi_m(\xi), \tag{42}$$

The appropriate solutions f_m, θ_m and φ_m corresponding to (f_m^*, θ_m^* and φ_m^*) are

$$f_m(\xi) = f_m^{?}(\xi) + A_1 + A_2 e^{\xi} + A_3 e^{-\xi},$$
$$\theta_m(\xi) = \theta_m^{?}(\xi) + A_4 e^{\xi} + A_5 e^{-\xi},$$
$$\varphi_m(\xi) = \varphi_m^{?}(\xi) + A_6 e^{\xi} + A_7 e^{-\xi}, \tag{43}$$

3.3. Convergence analysis

It is clear from the figure (see figure 1) $-1.5 \leqslant \hbar_f \leqslant -0.1$, $-1.4 \leqslant \hbar_\theta \leqslant -0.1$ and $-1.4 \leqslant \hbar_\varphi \leqslant -0.2$ are attained range values of auxiliary parameters $\hbar_f$, $\hbar_\theta$, and $\hbar_\varphi$ which represent the convergence region of the series solution. Well known Homotopic analysis technique is applied to get these ranges corresponding to velocity, temperature and concentration, the range, where plotted h-curves are horizontal indicated as convergence region.

4. Results and discussion

Temperature, velocity and concentration distributions are illustrated in this section. Figure 2 portrays the decreasing behavior of thermal buoyancy parameter λ on velocity profile $f'(\xi)$. It shows that velocity decays when λ increases. Physically, fluid convection due to gravity increases with the increment of λ which slows down the velocity profile. Figure 3 illustrates that larger ε (material fluid parameter) leads to larger horizontal velocity component. Physically, viscosity of fluid decreases against dominant ε and consequently velocity raises. Thus enhanced velocity field appears. Figure 4 exhibits role of β_1 (angle of inclination) on velocity field. Physically as the angle of inclination increases, velocity field also increases because buoyancy forces increase in the presence of gravitational force. Hence velocity field enhances. Figure 5 shows the conduct of temperature field due to the impact of Prandtl number. It describes that when Pr grows, temperature field decays. According to physical justification low thermal diffusivity is responsible for higher Prandtl number Pr which consequently results in less heat transfer from heated wall to cold fluid. Thus, decrement occurs in the fluid's temperature figure 6 depicts the character of R (radiation parameter) on temperature field $\theta(\xi)$. Infact larger R produces larger radiative heat flux on the surface which leads to higher temperature $\theta(\xi)$. Impact of δ_1 (heat generation/absorption parameter) on temperature enclosure $\theta(\xi)$ is displayed in figure 7. It has been found that with the increment of heat generation parameter more heat produces due to which temperature profile increases. Though opposite behavior of temperature field is found for heat absorption parameter. Character of temperature field due to thermal Biot number γ_1 is expressed in figure 8. As thermal Biot number increases, heat transfer rate increases and consequently temperature of the fluid grows. Behavior of solutal Biot number γ_2 on concentration profile is depicted in figure 9. Larger γ_2 corresponds to higher concentration field. Physically due to the increment of γ_2, mass transfer coefficient enhances and as a result concentration distribution enhances. Figure 10 elucidates characteristics of thermal stratification parameter S_1 on temperature field. It shows decreasing trend of temperature enclosure and related boundary layer. Physically, higher stratified parameter results in low convective flow between heated wall and ambient fluid. Thus, temperature field decays. Figure 11 reflects the impact of chemical reaction parameter kr on concentration field. Concentration field enhances for dominant values of costructive chemical reaction. For dominant constructive chemical reaction parameter, more fluid particles are produced as a product. Hence concentration field enhances. Figure 12 demonstrates impact of solutal stratification parameter S_2 on concentration field. Dominant S_2 is responsible for lower concentration. Infact larger S_2 reduces the concentration difference between concentration of the sheet and ambient fluid which behaves as a resistance for mass transfer. Hence, concentration field decays. Diversity in concentration distribution due to Sc is scrutinized in figure 13. Concentration field reflects decreasing behavior for larger Sc. It describes that because of low mass diffusion Sc raises, which results reduction in concentration enclosure. Figure 14 displays the impact of Prandtl number Pr on entropy generation. Entropy generation rate increases for dominant Pr. Fluids with higher Pr corresponding to lower thermal conductivity. Thus fluid has small temperature field and in more probable or equilibrium state. Hence entropy generation rate increases. Figure 15 demonstrates that there is an obvious enhancement in entropy generation rate corresponding to Eckert number Ec, Physically, difference between boundary layer enthalpy and kinetic energy of particles in flow increase which results enhancement in irreversibility rate, thus entropy generation rate increases. Figure 16 investigates the behavior of ε and solutal buoyancy parameter λ_1 on skin friction $Re_x^{1/2}Cf$. It is noticed that with the increment in ε and $\lambda 1$. Skin friction coefficient decays. Figure 17 displays the behavior of thermal stratification parameter S_1 and Prandtl number Pr on Nusselt number enclosure. It shows as S_1 and Pr grows Nusselt number rises. Figure 18 reveals the response of Schmidt number and chemical reaction parameter on Sherwood number. It is noticed that with the increment of Sc and kr Sherwood number gets boost.

Table 1 represents the comparison of skin friction with Wahab *et al* [33] and Javed *et al* [34]. It is concluded that all the results are in good agreement.

5. Summary

In present investigation phenomena of radiation and heat generation/absorption with nonlinear stratification in Powell–Eyring fluid flow in assistance with Entropy generation condition are analyzed and declared. The important points are summarized as:

- Angle of inclination executes gain in velocity field because of higher rate of transfer of heat.
- Radiation parameter concludes raise in temperature field due to higher heat flux on surface.
- Heat generation/absorption results increased temperature profile because of heat generation.
- Solutal and thermal Biot number are liable for higher concentration and temperature fields respectively.
- Thermal and solutal stratified parameter accordingly lessen the temperature and concentration fields respectively.
- Chemical reaction parameter boosts up the concentration field.
- Entropy generation increases with the increment of Prandtl number and Eckert number.

ORCID iDs

Iffat Jabeen https://orcid.org/0000-0003-3278-3460
S Ahmad https://orcid.org/0000-0002-4865-3161

References

[1] Khan M I, Ahmad S, Hayat T and Alsaedi A 2018 Entropy generation and activation energy impact on radiative flow of viscous fluid in presence of binary chemical reaction *Int. J. Chem. Reactor Eng.* **16** 20180045
[2] Khan M I, Qayyum S, Hayat T, Imran Khan M and Alsaedi A 2019 Entropy optimization in flow of Williamson nanofluid in the presence of chemical reaction and Joule heating *Int. J. Heat Mass Transfer* **133** 959–67
[3] Alharbi S O, Dawar A, Shah Z, Khan W, Idrees M, Islam S and Khan I 2018 Flow over an unsteady oscillatory porous stretching surface under the impact of thermal radiation and heat source/sink, entropy generation in MHD Eyring–Powell fluid *Appl. Sci.* **8** 2588
[4] Jamshed W and Aziz A 2018 A comparative entropy based analysis of Cu and Fe_3O_4/methanol Powell–Eyring nanofluid in solar thermal collectors subjected to thermal radiation, variable thermal conductivity and impact of different nanoparticles shape *Results Phys.* **9** 195–205
[5] Butt A S, Ali A and Mehmood A 2016 Entropy analysis in MHD nanofluid flow near a convectively heated stretching surface *Int. J. Exergy* **20** 318–42
[6] Butt A S, Ali A, Nazim T and Mehmood A 2017 Entropy production in mixed convective magnetohydrodynamic flow of nanofluid over a linearly stretching sheet *J. Nanofluids* **6** 379–89
[7] Butt A S, Ali A, Masood R and Hussain Z 2018 Parametric study of entropy generation effects in magnetohydrodynamic radiative flow of second grade nanofluid past a linearly convective stretching surface embedded in a porous medium *J. Nanofluids* **7** 1004–23
[8] Hayat T, Zubair M, Waqas M, Alsaedi A and Ayub M 2017 On doubly stratified chemically reactive flow of Powell–Eyring liquid subject to non-Fourier heat flux theory *Results Phys.* **7** 99–106
[9] Adesanyaa S O, Ogunseyeb H A and Jangilic S 2018 Unsteady squeezing flow of a radiative Eyring–Powell fluid channel flow with chemical reactions *Int. J. Therm. Sci.* **125** 440–7
[10] Rehman K, Malik M Y, Salahuddin T and Naseer M 2016 Dual stratified mixed convection flow of Eyring–Powell fluid over an inclined stretching cylinder with heat generation/absorption effect *AIP Adv.* **6** 2158–3226
[11] Rehman K, Malik M Y and Makinde O D 2018 Parabolic curve fitting study subject to Joule heating in MHD thermally stratified mixed convection stagnation point flow of Eyring–Powell fluid induced by an inclined cylindrical surface *J. King Saud Univ.—Sci.* **30** 440–9
[12] Rahimi J, Ganji D D, Khaki M and Hosseinzadeh K 2017 Solution of the boundary layer flow of an Eyring–Powell non-Newtonian fluid over a linear stretching sheet by collocation method *Alexandria Eng. J.* **56** 621–7
[13] Hayat T, Qayyum S, Shehzad S A and Alsaedi A 2018 Cattaneo–Christov double-diffusion theory for three-dimensional flow of viscoelastic nanofluid with the effect of heat generation/absorption *Results Phys.* **8** 489–95
[14] Hayat T, Qayyum S, Shehzad S and Alsaedi A 2017 Chemical reaction and heat generation/absorption aspects in flow of Walters-B nanofluid with Cattaneo–Christov double-diffusion *Results Phys.* **7** 4145–52
[15] Soomro F A, Haq R, Qasem M, Al-Mdallal M and Zhang Q 2018 Heat generation/absorption and nonlinear radiation effects on stagnation point flow of nanofluid along a moving surface *Results Phys.* **8** 404–14
[16] Qayyum S, Hayat T and Alsaedi A 2018 Thermal radiation and heat generation/absorption aspects in third grade magneto-nanofluid over a slendering stretching sheet with Newtonian conditions *Physica* B **537** 139–49
[17] Anjum A, Mir N A, Farooq M, Javed M, Ahmad S, Malik M Y and Alshomrani A S 2018 Physical aspects of heat generation/absorption in the second grade fluid flow due to Riga plate: application of Cattaneo–Christov approach *Results Phys.* **9** 955–60
[18] Liao. S J 2012 *Homotopy Analysis Method in Non-Linear Differential Equation* (Heidelberg: Springer and Higher Education Press)
[19] Liao S J 2014 *Advances in the Homotopy Analysis Method* (Singapore: World Scientific)
[20] Liao S J 2003 *Beyond Perturbation: Introduction to Homotopy Analysis Method* (London, Boca Raton, FL: Chapman and Hall, CRC Press)
[21] Ahmad S, Farooq M, Javed M and Anjum A 2018 Slip analysis of squeezing flow using doubly stratified fluid *Results Phys.* **9** 527–33
[22] Farooq M, Ahmad S, Javed M and Anjum A 2017 Analysis of Cattaneo–Christov heat and mass fluxes in the squeezed flow embedded in porous medium with variable mass diffusivity *Results Phys.* **7** 3788–96
[23] Ahmad S, Farooq M, Javed M and Anjum A 2018 Double stratification effects in chemically reactive squeezed Sutterby fluid flow with thermal radiation and mixed convection *Results Phys.* **8** 1250–9

[24] Jabeen I, Farooq M and Mir N A 2019 Variable mass and thermal properties in three-dimensional viscous flow: application of Darcy law *J. Cent. South Univ.* **26** 1271–82
[25] Gireesha B J, Gorla1 R S R and Mahanthesh B 2015 Effect of suspended nanoparticles on three-dimensional MHD Flow, heat and mass transfer of radiating Eyring–Powell fluid over a stretching sheet *J. Nanofluids* **4** 1–11
[26] Hayat T and Farooq M 2013 Melting heat transfer in the stagnation point flow of Powell–Eyring fluid *J. Thermophys. Heat Transfer* **27** 761–6
[27] Ramzan M, Farooq M, Hayat T and Chung J D 2016 Radiative and Joule heating e ects in the MHD ßow of a micropolar ßuid with partial slip and convective boundary condition *J. Mol. Liq.* **221** 394–400
[28] Jabeen I, Farooq M and Mir N A 2019 Description of stratification phenomena in the fluid reservoirs with first-order chemical reaction *Adv. Mech. Eng.* **11** 1–9
[29] Khan I, Fatima S, Malik M Y and Salahudd T 2018 Exponentially varying viscosity of magnetohydrodynamic mixed convection Eyring–Powell nanofluid flow over an inclined surface *Results Phys.* **8** 1194–203
[30] Bejan. A 2018 Thermodynamics today *Energy* **160** 1208–19
[31] Bejan. A 1987 The thermodynamic design of heat and mass transfer process and devices *Heat Fluid Flow* **8** 258–76
[32] Bejan. A 1979 A study of entropy generation in fundamental convective heat transfer *ASME J. Heat Transfer* **101** 718–25
[33] Wahab H A, Hussain1 S, Bhatti S and Naeem M 2016 Mixed convection flow of Powell–Eyring fluid over a stretching cylinder with Newtonian heating *Kuwait J. Sci.* **43** 1–13
[34] Javed T, Ali N, Abbas Z and Sajid M 2013 Flow of an Eyring–Powell non-Newtonian fluid over a stretching sheet *Chem. Eng. Commun.* **200** 327–36